LETTERS
https://doi.org/10.1038/s41567-018-0313-7

nature physics

A photon–photon quantum gate based on Rydberg interactions

Daniel Tiarks, Steffen Schmidt-Eberle, Thomas Stolz, Gerhard Rempe and Stephan Dürr*

The interaction between Rydberg states of neutral atoms is strong and long-range, making it appealing to put it to use in the context of quantum technologies. Recently, first applications of this idea have been reported in the fields of quantum computation[1] and quantum simulation[2–4]. Furthermore, electromagnetically induced transparency allows one to map these Rydberg interactions to light[5–15]. Here we exploit this mapping and the resulting interaction between photons to realize a photon–photon quantum gate[16,17], demonstrating the potential of Rydberg systems as a platform also for quantum communication and quantum networking[18]. We measure a controlled-NOT truth table with a fidelity of 70(8)% and an entangling-gate fidelity of 63.7(4.5)%, both post-selected upon detection of a control and a target photon. The level of control reached here is an encouraging step towards exploring novel many-body states of photons or for future applications in quantum communication and quantum networking[18].

Optical technologies serve as today's standard for distributing information in the Internet, since photons offer high speed and large bandwidth. Because of these benefits, future quantum technologies will probably rely on photonic qubits to transfer quantum states between distant nodes. However, ambitions to use photons for processing rather than only transmitting qubits are hampered by the fact that photons hardly interact with each other. A solution to this problem is offered by a Rydberg polariton[6–15]. This intriguing quasiparticle—composed of a photonic component and an atomic Rydberg excitation—is obtained when a photon enters a medium in which electromagnetically induced transparency (EIT) couples the photon to a Rydberg state. The key idea is that the strong, long-range interaction between the atomic Rydberg components is mapped onto the photons. The potential for applying this to build a photon–photon gate has been discussed at great length in the literature. The importance of this goal can be illustrated by the large number of schemes proposed for building a Rydberg-based photon–photon quantum gate[6,7,19–26]. In addition, the demonstration of a photon–photon quantum gate is the hallmark for having achieved full quantum control of one photon over another.

Here we report on the first experimental demonstration of a Rydberg-based photon–photon quantum gate. An important ingredient is the creation of a conditional π phase shift. To achieve this, first, a control photon is stored in an ultracold atomic ensemble based on EIT, in such a way that the left- and right-handed circular polarizations $|L\rangle$ and $|R\rangle$ are stored in a Rydberg state $|69S\rangle$ and a ground state $|g'\rangle$, respectively (Fig. 1 and Methods). Second, a target photon propagates through the ensemble. Its $|L\rangle$ polarization is coupled to another Rydberg state $|67S\rangle$ by EIT, making it a Rydberg polariton, whereas its $|R\rangle$ polarization simply propagates off-resonantly through the ensemble. Only if both photons have $|L\rangle$ polarization, will they both have a Rydberg component, causing them to interact. This interaction modifies the linear electric susceptibility χ experienced by the target photon. And that modifies the phase shift that the target photon accumulates during propagation through the ensemble. For appropriate parameters the resulting conditional phase shift equals π. Finally, the control photon is retrieved. This realizes a controlled phase flip gate. A change of basis easily converts this into a controlled-NOT (CNOT) gate.

Each incoming qubit is implemented as an attenuated pulse of laser light with Poissonian photon number statistics and mean photon number below unity. Data are post-selected upon detection of one photon in each pulse to compensate for non-unity efficiencies and for the photon statistics of the input. The efficiency of the gate (that is, the probability that the atomic ensemble transmits a photon pair impinging on it) ranges between 8% and 0.5%, depending on input polarizations.

In our experiment, the conditional π phase shift is accumulated from the interaction of the two wavepackets during their spatiotemporal overlap. This is a long-standing goal since the 1980s, where it was the basis for the first proposal for a quantum gate for photons[27]. Previous experimental realizations of photon–photon quantum gates circumvented the difficulty in creating an interaction between overlapping wave packets. As a workaround, they relied either on linear optics combined with inherently probabilistic protocols[16] or on a sequence of two atom–photon gates[17].

We previously demonstrated[13] one important ingredient of the gate, namely a conditional phase shift $\Delta\beta$ of π. The present experiment features two crucial advances that make it possible to realize a quantum gate. First, achieving high post-selected fidelity requires that the conditional optical depth ΔOD vanishes because the ideal gate has vanishing ΔOD and single-qubit operations cannot change ΔOD (Methods). When trying to simultaneously reach $\Delta\beta=\pi$ and $\Delta\mathrm{OD}=0$, the main limiting factor is dephasing (that is, decay of coherence between the ground state $|g\rangle$ and the Rydberg state $|67S\rangle$). This makes it nontrivial to find suitable experimental parameters (Methods).

Second, in previous work[13] we conditioned the π phase shift on the presence or absence of a control photon to be stored in state $|69S\rangle$. The presence or absence of a photon represents a qubit, but using the qubit in this form is inexpedient in an experiment because photon loss will cause bit-flip errors and because single-qubit unitaries are difficult to realize. We solve this problem by mapping this qubit onto a polarization qubit so that photon loss can be handled by post-selection and single-qubit unitaries are easy to implement using waveplates. The $|L\rangle$ polarization of the qubit is stored in state $|69S\rangle$. As the $|L\rangle$ and $|R\rangle$ polarizations of this qubit must interfere at the detector, the $|R\rangle$ polarization must be delayed as much as the stored $|L\rangle$ polarization. In principle, this could be achieved in several ways (Methods). We choose to store the $|R\rangle$ polarization in

Max-Planck-Institut für Quantenoptik, Garching, Germany. *e-mail: stephan.duerr@mpq.mpg.de

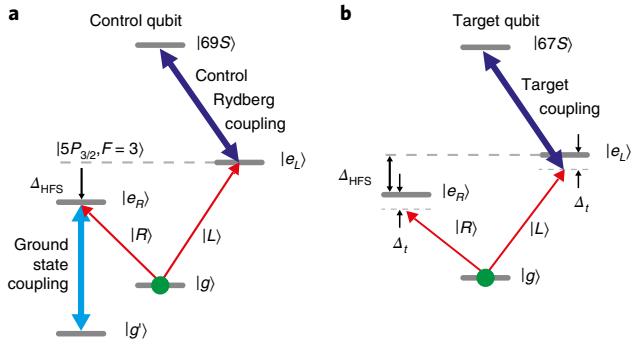

Fig. 1 | Atomic level schemes. a, Level scheme for EIT storage of the control qubit. The initial population (green) is prepared in state $|g\rangle$. $|L\rangle$ polarization is stored in a Rydberg state $|69S\rangle$, $|R\rangle$ polarization in a ground state $|g'\rangle$. **b**, Level scheme for the target qubit. $|L\rangle$ polarization propagates as a Rydberg polariton involving Rydberg state $|67S\rangle$, $|R\rangle$ polarization propagates off-resonantly without experiencing EIT.

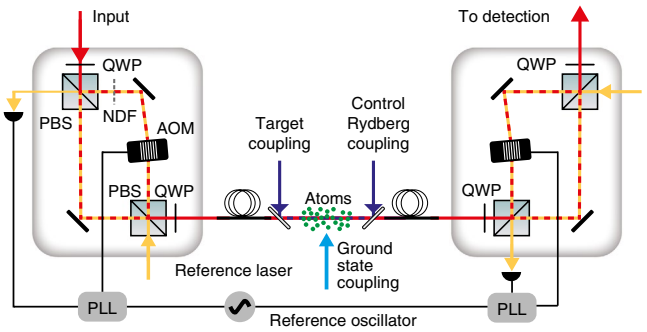

Fig. 2 | Simplified scheme of the experimental set-up. The control photon (red) passes through a first interferometer (left box), interacts with the atomic ensemble (green), and finally passes through a second interferometer (right box). The first interferometer shifts the frequency of only the $|R\rangle$ polarization by $\Delta_{HFS}/2\pi$. The second interferometer removes this frequency shift. Counterpropagating reference light (yellow) and phase-locked loops (PLLs) stabilize each interferometer against thermal drift. Coupling light (blue, cyan) establishes EIT. The target photon takes the same path as the control photon.

the $|g'\rangle = |5S_{1/2}, F = m_F = 1\rangle$ ground state, where F and m_F are the hyperfine quantum numbers.

For reasons discussed in the Methods, we choose the frequency of the incoming control photon to be resonant with the $|g\rangle \leftrightarrow |5P_{3/2}, F = 3\rangle$ transition (Fig. 1a). As a result, achieving storage in state $|g'\rangle$ is not straightforward because the states $|g'\rangle$ and $|5P_{3/2}, F = 3\rangle$ are not connected by an electric-dipole transition because of $\Delta F = 2$. We overcome this hurdle by frequency shifting selectively only the $|R\rangle$ component of the control photon to make it resonant with the transition from $|g\rangle$ to $|e_R\rangle = |5P_{3/2}, F = 2, m_F = 1\rangle$. From here, we achieve resonant EIT-based storage in $|g'\rangle$. To create the required frequency shift of $\Delta_{HFS}/2\pi = 267$ MHz, we use an acousto-optic modulator (AOM). To shift the frequency of only one polarization, we first spatially split the polarizations with a quarter-wave plate (QWP) and a polarizing beam splitter (PBS), send only one of the beams through the AOM, and finally recombine the beams using another PBS and QWP. Overall, this realizes a modified Mach–Zehnder interferometer that creates a frequency shift for only the $|R\rangle$ polarization (left half of Fig. 2).

The storage is achieved by simultaneously switching off both control coupling light fields while the control photon is inside the medium. After a dark time set to 4.5 μs, both control coupling light fields are simultaneously switched back on and both polarization components of the control qubit are retrieved. To remove the frequency shift of the $|R\rangle$ component, the retrieved light is sent through a similar interferometer (right half of Fig. 2). Overall, this realizes an EIT-based quantum memory, which is sophisticated insofar as this memory stores one polarization component in a Rydberg state and the other in a ground state. This has the decisive advantage that only the Rydberg component will strongly interact with the target photon when it propagates through the medium during the dark time, thus making a quantum gate possible. The average post-selected fidelity[28] of the quantum memory is $F_m = 87.5(7)\%$ (Supplementary Information), which clearly exceeds the classical limit 2/3.

To build a photon–photon gate, we combine this quantum memory for the control qubit with the conditional π phase shift of the target photon, as described above. On top of that, there are single-qubit phase shifts (Methods), which we choose such that the complete gate operation should ideally yield a truth table $|RR\rangle \mapsto |RR\rangle$, $|RL\rangle \mapsto -|RL\rangle$, $|LR\rangle \mapsto |LR\rangle$ and $|LL\rangle \mapsto |LL\rangle$, where the control qubit is listed first. This constitutes a controlled phase flip gate, which is a universal two-qubit gate.

We now turn to the characterization of this gate. Figure 3a shows a measured CNOT truth table in which the first photon is initially in the horizontal $|H\rangle = (|R\rangle + |L\rangle)/\sqrt{2}$ or vertical $|V\rangle = i(|R\rangle - |L\rangle)/\sqrt{2}$ polarization state, whereas the second photon is initially in $|R\rangle$ or $|L\rangle$. The fidelity of this post-selected truth table (that is, the probability of obtaining the desired output averaged over all four input states) is $F_{CNOT} = 70(8)\%$. Figure 3b shows a similar CNOT truth table but with the input polarizations of the first and second photon swapped, yielding $F_{CNOT} = 66(9)\%$. Studying the performance of both versions of the CNOT gate is interesting because the photons are treated differently insofar as one is stored and retrieved, whereas the other propagates without storage.

To demonstrate that the gate operates in the quantum regime, we study an entangling-gate operation. To this end, we prepare the input state $|HH\rangle$. From this, the gate should ideally produce the maximally entangled output state $|\psi_i\rangle = (|LH\rangle - i|RV\rangle)/\sqrt{2}$. The actual output state can be described by a density matrix ρ. We measure a post-selected fidelity of $F_e = \langle\psi_i|\,\rho\,|\psi_i\rangle = 63.7(4.5)\%$ (linear unbiased estimator). This is well above the threshold of 1/2 for demonstrating entanglement. Using quantum state tomography, we reconstruct the density matrix ρ (linear unbiased estimator) (Fig. 3c,d). We note that in a simple model (Supplementary Information), the non-unity visibilities of the control qubit and the target qubit already set an upper bound of 76(6)% to F_e. The difference between the measured value and this upper bound indicates that there are additional imperfections in the gate operation beyond the single-qubit visibilities (Supplementary Information).

The above results demonstrate the first realization of a Rydberg-based photon–photon quantum gate. It is a clear advantage of the gate scheme used here that its implementation requires manageable experimental effort. However, when aiming at high fidelity and high efficiency, other schemes[6,7,19–26] might be better suited; an excitation-hopping-based approach[15] at present seems to yield similar efficiency (Supplementary Information). Nevertheless, we believe that the efficiency and fidelity of the present scheme can both be improved. For example, EIT storage and retrieval with an efficiency of 92% has been achieved recently[29]. Future improvements in efficiency and fidelity might make high-efficiency photonic Bell state detection possible, which is crucial for quantum repeaters. Once efficiency and fidelity are improved, the present scheme could be extended to the generation of entangled states of several photonic qubits, by transmitting more than one target photon in the presence of the same stored control photon. Additionally, Rydberg-based quantum gates might allow for miniaturization and transfer

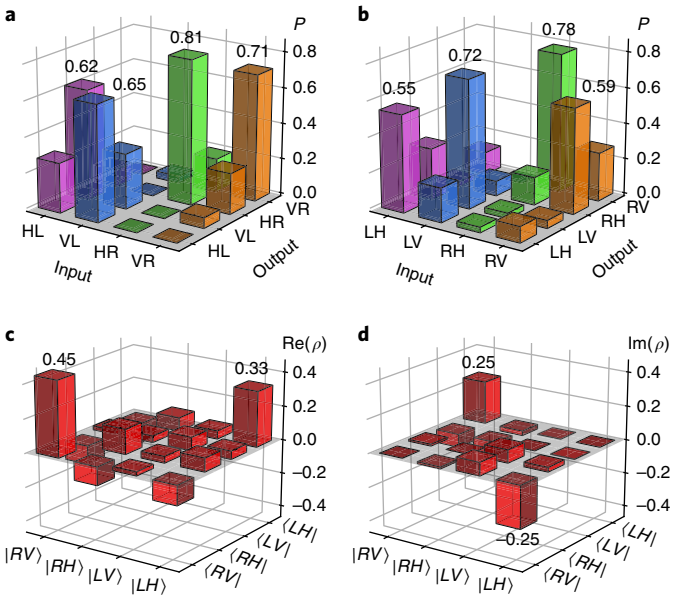

Fig. 3 | Performance of the photon-photon gate. a, Truth table of the CNOT gate operation. To obtain a truth table, one of the four displayed input states is prepared repeatedly and the probability P to obtain the displayed output states is measured. Ideally, the polarizations $|H\rangle$ and $|V\rangle$ of the first qubit should be exchanged if and only if the second qubit is in $|L\rangle$. **b**, Same as in **a** but with the input polarizations of the first and second qubit swapped. **c**,**d**, Real (**c**) and imaginary (**d**) parts of the reconstructed density matrix ρ of the two-photon state created in the entangling-gate operation.

to solid-state systems. For example, interactions between Rydberg excitons in a solid have been observed recently[30].

Online content

Any methods, additional references, Nature Research reporting summaries, source data, statements of data availability and associated accession codes are available at https://doi.org/10.1038/s41567-018-0313-7.

Received: 13 July 2018; Accepted: 12 September 2018;
Published online: 29 October 2018

References

1. Saffman, M. Quantum computing with atomic qubits and Rydberg interactions: progress and challenges. *J. Phys. B* **49**, 202001 (2016).
2. Schauß, P. et al. Crystallization in Ising quantum magnets. *Science* **347**, 1455–1458 (2015).
3. Labuhn, H. et al. Tunable two-dimensional arrays of single Rydberg atoms for realizing quantum Ising models. *Nature* **534**, 667–670 (2016).
4. Bernien, H. et al. Probing many-body dynamics on a 51-atom quantum simulator. *Nature* **551**, 579–584 (2017).
5. Lukin, M. D. et al. Dipole blockade and quantum information processing in mesoscopic atomic ensembles. *Phys. Rev. Lett.* **87**, 037901 (2001).
6. Friedler, I., Petrosyan, D., Fleischhauer, M. & Kurizki, G. Long-range interactions and entanglement of slow single-photon pulses. *Phys. Rev. A* **72**, 043803 (2005).
7. Gorshkov, A. V., Otterbach, J., Fleischhauer, M., Pohl, T. & Lukin, M. D. Photon–photon interactions via Rydberg blockade. *Phys. Rev. Lett.* **107**, 133602 (2011).
8. Pritchard, J. D. et al. Cooperative atom–light interaction in a blockaded Rydberg ensemble. *Phys. Rev. Lett.* **105**, 193603 (2010).
9. Firstenberg, O. et al. Attractive photons in a quantum nonlinear medium. *Nature* **502**, 71–75 (2013).
10. Baur, S., Tiarks, D., Rempe, G. & Dürr, S. Single-photon switch based on Rydberg blockade. *Phys. Rev. Lett.* **112**, 073901 (2014).
11. Gorniaczyk, H., Tresp, C., Schmidt, J., Fedder, H. & Hofferberth, S. Single-photon transistor mediated by interstate Rydberg interactions. *Phys. Rev. Lett.* **113**, 053601 (2014).
12. Tiarks, D., Baur, S., Schneider, K., Dürr, S. & Rempe, G. Single-photon transistor using a Förster resonance. *Phys. Rev. Lett.* **113**, 053602 (2014).
13. Tiarks, D., Schmidt, S., Rempe, G. & Dürr, S. Optical π phase shift created with a single-photon pulse. *Sci. Adv.* **2**, 1600036 (2016).
14. Ningyuan, J. et al. Observation and characterization of cavity Rydberg polaritons. *Phys. Rev. A* **93**, 041802 (2016).
15. Thompson, J. D. et al. Symmetry-protected collisions between strongly interacting photons. *Nature* **542**, 206–209 (2017).
16. O'Brien, J. L., Pryde, G. J., White, A. G., Ralph, T. C. & Branning, D. Demonstration of an all-optical quantum controlled-NOT gate. *Nature* **426**, 264–267 (2003).
17. Hacker, B., Welte, S., Rempe, G. & Ritter, S. A photon–photon quantum gate based on a single atom in an optical resonator. *Nature* **536**, 193–196 (2016).
18. Kimble, H. J. The quantum internet. *Nature* **453**, 1023–1030 (2008).
19. He, B., Sharypov, A. V., Sheng, J., Simon, C. & Xiao, M. Two-photon dynamics in coherent Rydberg atomic ensemble. *Phys. Rev. Lett.* **112**, 133606 (2014).
20. Paredes-Barato, D. & Adams, C. S. All-optical quantum information processing using Rydberg gates. *Phys. Rev. Lett.* **112**, 040501 (2014).
21. Khazali, M., Heshami, K. & Simon, C. Photon–photon gate via the interaction between two collective Rydberg excitations. *Phys. Rev. A* **91**, 030301 (2015).
22. Hao, Y. M. et al. Quantum controlled-phase-flip gate between a flying optical photon and a Rydberg atomic ensemble. *Sci. Rep.* **5**, 10005 (2015).
23. Das, S. et al. Photonic controlled-PHASE gates through Rydberg blockade in optical cavities. *Phys. Rev. A* **93**, 040303 (2016).
24. Wade, A. C. J., Mattioli, M. & Mølmer, K. Single-atom single-photon coupling facilitated by atomic-ensemble dark-state mechanisms. *Phys. Rev. A* **94**, 053830 (2016).
25. Murray, C. R. & Pohl, T. Coherent photon manipulation in interacting atomic ensembles. *Phys. Rev. X* **7**, 031007 (2017).
26. Lahad, O. & Firstenberg, O. Induced cavities for photonic quantum gates. *Phys. Rev. Lett.* **119**, 113601 (2017).
27. Milburn, G. J. Quantum optical Fredkin gate. *Phys. Rev. Lett.* **62**, 2124–2127 (1989).
28. Bowdrey, M. D., Oi, D. K. L., Short, A. J., Banaszek, K. & Jones, J. A. Fidelity of single qubit maps. *Phys. Lett. A* **294**, 258–260 (2002).
29. Hsiao, Y.-F. et al. Highly efficient coherent optical memory based on electromagnetically induced transparency. *Phys. Rev. Lett.* **120**, 183602 (2018).
30. Kazimierczuk, T., Fröhlich, D., Scheel, S., Stolz, H. & Bayer, M. Giant Rydberg excitons in the copper oxide Cu_2O. *Nature* **514**, 343–347 (2014).

Acknowledgements

This work was supported by Deutsche Forschungsgemeinschaft through Nanosystems Initiative Munich.

Author contributions

All authors contributed extensively to the work presented here.

Competing interests

The authors declare no competing interests.

Additional information

Supplementary information is available for this paper at https://doi.org/10.1038/s41567-018-0313-7.

Reprints and permissions information is available at www.nature.com/reprints.

Correspondence and requests for materials should be addressed to S.D.

Publisher's note: Springer Nature remains neutral with regard to jurisdictional claims in published maps and institutional affiliations.

Methods

Atomic transitions. The experiment begins with the preparation of a gas of typically 10^5 ultracold ^{87}Rb atoms at a temperature of typically 0.6 μK in an optical dipole trap (Supplementary Information). The internal state is prepared in the $|g\rangle = |5S_{1/2}, F = m_F = 2\rangle$ ground state.

The incoming control photon is resonant with the $|g\rangle \leftrightarrow |5P_{3/2}, F = 3\rangle$ transition at a wavelength of 780 nm. The $|L\rangle$ polarization of this photon is stored in the Rydberg state $|69S\rangle = |69S_{1/2}, F = m_F = 2\rangle$ based on resonant Rydberg EIT using control Rydberg coupling light at 480 nm and the intermediate state $|e_L\rangle = |5P_{3/2}, F = m_F = 3\rangle$. The $|R\rangle$ polarization of the control photon is stored in the ground state $|g'\rangle = |5S_{1/2}, F = m_F = 1\rangle$ based on resonant EIT using ground-state coupling light at 780 nm and the intermediate state $|e_R\rangle = |5P_{3/2}, F = 2, m_F = 1\rangle$ (Fig. 1a and Supplementary Information). To make the latter possible, the $|R\rangle$ polarization of the control photon is frequency shifted using the modified Mach–Zehnder interferometer discussed above. In addition, this frequency shift creates a large detuning from the Rydberg-EIT resonance, thus preventing undesired storage of the $|R\rangle$ polarization in a Rydberg state.

The incoming target photon is detuned by $\Delta_t/2\pi = -17$ MHz (to the red) from the $|g\rangle \leftrightarrow |e_L\rangle$ resonance. The $|L\rangle$ polarization of this photon propagates through the medium as a Rydberg polariton, experiencing Rydberg EIT with intermediate state $|e_L\rangle$ (Fig. 1b) and with Rydberg state $|67S\rangle = |67S_{1/2}, F = m_F = 2\rangle$, which features a Förster resonance with the $|69S\rangle$ state[12]. The target photon takes the same beam path through the set-up as the control photon. In particular, it also passes through both interferometers. Hence, the $|R\rangle$ polarization of the target photon, which enters the set-up at the same frequency as the $|L\rangle$ polarization, is $-\Delta_{\mathrm{HFS}}/2\pi = -267$ MHz detuned from the two-photon resonance for Rydberg EIT when reaching the atoms. This means that the $|R\rangle$ polarization does not experience EIT. Instead, its dominant interaction with the medium comes from the $|g\rangle \leftrightarrow |e_R\rangle$ transition, from which it is detuned by −17 MHz.

Phase shifts and photon loss. The combination of propagation, storage, and retrieval changes the polarization state $|j\rangle$ of the control photon with $j \in \{R, L\}$ to $\mathrm{e}^{-\mathrm{OD}_{c,j}/2 + i\beta_{c,j}}\ |j\rangle$, where $\beta_{c,j}$ is the accumulated phase shift and $\mathrm{OD}_{c,j}$ expresses photon loss. We choose to operate the incoming control photon and both control coupling lasers at the single-photon resonances because this should minimize loss of the control photon. Theoretically, this should automatically yield $\beta_{c,L} - \beta_{c,R} = 0$. In practice, we fine tune the frequency of one of the control coupling lasers to achieve $\beta_{c,L} - \beta_{c,R} = 0$ for all dark times.

Propagation through the medium in the absence of a control qubit changes the polarization state $|j\rangle$ of the target photon with $j \in \{R, L\}$ to $\mathrm{e}^{-\mathrm{OD}_j/2 + i\beta_j}\ |j\rangle$, where β_j is the accumulated phase shift and OD_j the optical depth. The $|g\rangle \leftrightarrow |e_R\rangle$ transition has a relatively small electric dipole matrix element, making its resonant optical depth a factor of six smaller than for the $|g\rangle \leftrightarrow |e_L\rangle$ transition. Hence, the polarization $|R\rangle$ experiences relatively high transmission $\mathrm{e}^{-\mathrm{OD}_R} \sim 0.77$ and a phase shift $\beta_R \sim 0.9$ rad, which is of little relevance.

If a control qubit is stored in Rydberg state $|69S\rangle$, then Rydberg blockade modifies the linear electric susceptibility χ experienced by the $|L\rangle$ polarization of the target qubit. This changes the values of OD_L and β_L to OD_{LL} and β_{LL}, respectively. The conditional optical depth is $\Delta\mathrm{OD} = \mathrm{OD}_{LL} - \mathrm{OD}_L$ and the conditional phase shift $\Delta\beta = \beta_{LL} - \beta_L$. The control qubit affects neither OD_R nor β_R. Although $\Delta_t = 0$ would be a good choice if one aimed for large ΔOD combined with $\Delta\beta = 0$, we choose a value of $|\Delta_t|$ which is quite a bit larger than the natural linewidth $\Gamma_e = 2\pi \times 6$ MHz of state $|e_L\rangle$ because we instead aim for $\Delta\mathrm{OD} = 0$ combined with a large value of $\Delta\beta$ (Supplementary Information).

Zeroing the conditional optical depth ΔOD is important for achieving a high post-selected fidelity of the gate. To see this, assume that we attempt to create the entangled state $|\psi_i\rangle = (|LH\rangle - i\ |RV\rangle)\ /\ \sqrt{2}$ but instead obtain the normalized output state

$$|\psi_\xi\rangle = \frac{1}{2}\mathrm{e}^{-\xi_0}(|RR\rangle + \mathrm{e}^{-\xi_2}\ |RL\rangle + \mathrm{e}^{-\xi_1}\ |LR\rangle + \mathrm{e}^{-\xi_1-\xi_2-\xi_3}\ |LL\rangle) + c_{\mathrm{abs}}\ |\psi_{\mathrm{abs}}\rangle \qquad (1)$$

Here the normalized state vector $|\psi_{\mathrm{abs}}\rangle$ with a complex amplitude c_{abs} contains all those components of the state that correspond to absorption of at least one photon. Hence, $|\psi_{\mathrm{abs}}\rangle$ is orthogonal to the states $|RR\rangle$, $|RL\rangle$, $|LR\rangle$ and $|LL\rangle$. When finally post-selecting upon detection of one control and one target photon, then all other properties of $|\psi_{\mathrm{abs}}\rangle$ become irrelevant, so it is unnecessary to detail them here. $1 - |c_{\mathrm{abs}}|^2$ is the probability that the state contains two photons.

All other coefficients are expressed in terms of the complex numbers ξ_i. A post-selected fidelity of unity would be achieved for $\xi_1 = 0$ and $\xi_2 = \xi_3 = i\pi$ along with arbitrary ξ_0. We decompose the ξ_i as $\mathrm{Re}(\xi_i) = \mathrm{OD}_i/2$ and $\mathrm{Im}(\xi_i) = -\beta_i$. The resulting phase shifts β_i are obviously related to the phase shifts discussed above, namely $\beta_1 = \beta_{c,L} - \beta_{c,R}$ and $\beta_2 = \beta_L - \beta_R$ are the differential phase shifts of the control and target qubit, respectively, $\beta_3 = \Delta\beta$ is the conditional phase shift, and $\beta_0 = \beta_R + \beta_{c,R}$ is a global phase shift, which is of little relevance. The interpretation of the OD_i is analogous, in particular $\mathrm{OD}_3 = \Delta\mathrm{OD}$.

It is a crucial point that using linear optics, including polarization-selective attenuators, it is experimentally easy to implement arbitrary single-qubit operations, as long as they maintain or attenuate intensities. If they act only on the first (second) qubit they will modify only ξ_0 and ξ_1 (ξ_0 and ξ_2). However, single-qubit operations can never modify ξ_3. To modify ξ_3, one needs interactions between the two qubits, which in our experiment result from Rydberg blockade during the passage of the target photon through the atomic ensemble. Hence, any undesired value of ξ_1 or ξ_2 that might be created when the photons pass through the atomic ensemble can be compensated before or after that passage with easy-to-implement single-qubit operations. But possible deviations from $\Delta\beta = \pi$ or $\Delta\mathrm{OD} = 0$ incurred during passage through the atomic ensemble cannot be compensated before or after that passage. This is why we aim to achieve $\Delta\beta = \pi$ and $\Delta\mathrm{OD} = 0$ simultaneously upon passage through the atomic ensemble.

In our experiment, the single-qubit operations needed to compensate $\mathrm{OD}_1 \neq 0$ and $\mathrm{OD}_2 \neq 0$ are easily implemented as follows. For the control qubit, $\mathrm{OD}_1 \neq 0$ is compensated by placing an appropriate neutral density filter (NDF) into one arm of the first interferometer. As $\mathrm{OD}_1 \neq \mathrm{OD}_2$, we additionally temporally switch the radiofrequency (rf) power driving the AOM in the first interferometer to obtain the appropriate compensation for the target qubit. At fixed optical input power, this implementation would reduce the overall count rate, but in our experiment it does not because we can increase the input power. This is because to avoid a degradation of the post-selected fidelity, the mean photon number per pulse impinging on the atomic ensemble must be below unity. Otherwise possible excess photons might become entangled with the other photons, and if the excess photons happen not to be detected, the post-selected fidelity deteriorates. The first interferometer, however, contains only linear optical elements. They cannot produce entanglement with the excess photons, so that loss of possible excess photons in the first interferometer has no effect on the post-selected fidelity.

Choice of parameter values. In the experiment, we need to choose a large number of parameters. A large principal quantum number has the advantage of yielding a large van der Waals coefficient C_6, which results in a large blockade radius r_b that in turn makes $\Delta\beta$ large. On the other hand, a large principal quantum number tends to yield a large dephasing rate γ_{rg}, which is undesirable. This motivates the choice of the Förster resonance between the Rydberg states $|67S\rangle$ and $|69S\rangle$ in ^{87}Rb, which increases $|C_6|$ by a factor of ~60 compared to $|69S\rangle$ and $|69S\rangle$[12].

In the presence of a nonzero dephasing rate γ_{rg}, the parameter regime in which $\Delta\beta = \pi$ and $\Delta\mathrm{OD} = 0$ can be achieved simultaneously is limited (Supplementary Information). In particular, it is advantageous to choose a transition for the $|L\rangle$ polarization of the target qubit, which has a large electric dipole matrix element. The largest electric dipole matrix element in an optical excitation from the 5S ground state is the one on the cycling transition $|g\rangle \leftrightarrow |e_L\rangle$. This is why we choose this transition for the target photon. Hence, the internal atomic state must initially be $|g\rangle$.

We want the frequency of the incoming control and target photons to be roughly the same, so that the control photon should also be near resonant with the $5S \leftrightarrow 5P$ transition. With the atomic population initially prepared in state $|g\rangle$, the $|L\rangle$ polarization of the control photon must use the same transition as the target photon, because the other fine- and hyperfine-structure components of the 5P state do not have $m_F = 3$ components. The disadvantage of this choice of transitions is that without selectively frequency shifting the $|R\rangle$ polarization, one cannot easily achieve storage of the $|R\rangle$ polarization in the $F = 1$ ground state.

In principle, one could alternatively store the $|R\rangle$ polarization in a Rydberg state with yet a different principal quantum number (for example, 68S). In terms of technical effort, this would require setting up a third 480 nm laser. This scenario would have the disadvantage of reducing $\Delta\beta$ because a stored $|R\rangle$ photon could also create Rydberg blockade for the target photon. As the C_6 coefficients will typically differ, $\Delta\beta$ would not vanish completely, but a substantial reduction in $\Delta\beta$ could already be a significant problem. Another alternative option could be to delay the $|R\rangle$ polarization in an optical fibre. This would require an active stabilization of the optical path length difference, resulting in a technical effort similar to the stabilization of the modified Mach–Zehnder interferometers. The two interferometers used in our set-up offer the advantage that the optical path length which must be stabilized does not contain the ultracold atomic gas, which could otherwise make the stabilization technically more challenging. Another advantage of the two interferometers is that the rf power of the AOM can be switched to compensate $\mathrm{OD}_1 \neq \mathrm{OD}_2$, as discussed above.

We typically choose an atomic peak density of $\rho = 2 \times 10^{12}\,\mathrm{cm}^{-3}$ and a length of the medium of $L = 60$ μm, similar to ref.[13]. The choice of ρ reflects a compromise. On the one hand, large ρ is preferable because it increases $\Delta\beta$ and storage efficiency. On the other hand, small ρ reduces the dephasing rate γ_{rg} (ref. [10]). The choice of L also reflects a compromise. On the one hand, large L is preferable because it increases storage efficiency and target photon visibility (Supplementary Information). On the other hand, small L reduces absorption loss during propagation. The dephasing rate γ_{rg} describes a decay of coherence between states

$|g\rangle$ and $|r\rangle = |67S\rangle$. For the density and principal quantum number used here, we typically measure $\gamma_{rg} = 1\,\mu s^{-1}$ (Supplementary Information). With these parameters, a detailed model (Supplementary Information) can be used to calculate optimal values for the coupling Rabi frequency Ω_{L1} and the signal detuning $\Delta_1/2\pi$, which we implement to a good approximation in our experiment.

With these choices, we carefully zero ΔOD by fine tuning the target two-photon detuning to be slightly off from the two-photon resonance (Supplementary Information). In addition, we carefully fine tune the combination of atom number and length of the medium to achieve $\Delta\beta = \pi$ and $\beta_2 = \pi$. The latter choice is motivated in the Supplementary Information.

Data availability

The data that support the plots within this paper and other findings of this study are available from the corresponding author upon reasonable request.